Role of Nanochemical Environments in Porous TiO_2 in Photocurrent Efficiency and Degradation in Dye Sensitized Solar Cells

Matthias Junghänel* and Helmut Tributsch

Department Solare Energetik, Hahn-Meitner-Institut, 14109 Berlin, Germany

Received: August 9, 2005; In Final Form: September 21, 2005

Elongated dye sensitized solar cells with a thickness gradient of the nanoporous TiO_2 front electrode were used to assess the impact of the layer thickness on photocurrent and degradation. The photocurrent efficiency passes through a maximum (in our case at about 12 μm). Interestingly, the degradation rate also strongly depends on the layer thickness and is about 3 times faster for a 15-μm cell (in comparison with a 1-μm cell). To explain these nonanticipated results, a model to describe the I_3^-/I^- concentration within a typical dye sensitized solar cell under steady-state conditions was derived. It includes the nanoporous TiO_2 layer and a bulk solution with their different mobilities for the electrolyte species. Using typical parameters from the literature, it turned out that, despite the fact that the initial I^- concentration is about 1 order of magnitude larger and the assumed diffusion coefficient is 1.3 times higher, the depletion of the I^- concentration at the TiO_2/FTO front contact happens to be in the same range as the depletion of the I_3^- concentration at the back contact. This stresses the importance of iodide in nanoporous environments for both the maximum attainable photocurrent and its role in the regeneration of the oxidized dye. Enhanced degradation rates might be related to poor iodide supply, since the oxidized state cannot be regenerated efficiently.

1. Introduction

Nanostructured dye sensitization solar cells (DSSCs) have received significant attention,[1−3] and over the years, much knowledge has been accumulated on various aspects of cell function. These especially include sensitizer function,[4−5] electrolyte composition,[6−8] charge migration in the nanoporous structure,[9,10] and the structure[11,12] and composition of the oxide matrix.[13−14] The operation principle is shown in Figure 1: the dye S, chemically attached on a TiO_2 matrix, injects electrons into the conduction band of TiO_2 upon excitation by incident photons. It is regenerated by a redox mediator (typically I_3^-/I^-), which controls the charge transport between the dye and the back-electrode.

The flux of the redox species in the electrolyte is believed to be mainly diffusional. The contribution of migration has been proven to be not significant,[15,16] and convection may only play a role in the bulk solution. A newly proposed Grotthuss-type mechanism was found to enhance charge transport in gel electrolyte DSSCs.[17] It is assumed that charge is simply transported by chemical bond exchange between I^- and higher polyiodides (I_3^-, I_5^-, ...). Yet, considering the relatively large distance of 10 Å between each iodide molecule (0.5 M, ionic radius 2.2 Å) and of 120 Å for iodide (0.05 M, ionic radius 1.3 Å), this mechanism can only accelerate the transport at a point where both redox species are in close proximity to each other, which seems to not be the case for typically used concentrations. So far, it has not been demonstrated that the charge transport in a liquid electrolyte DSSC can be enhanced by bond exchange. This mechanism has been suggested to explain high photocurrent densities of 40 mA/cm^2 under 500 mW/cm^2 of illumination.[18] For a purely diffusional model, the maximum attainable photocurrent is about 25 mA/cm^2, depending on the parameters used.

Up to now, theoretical description of the I_3^- transport have been mainly done by Ferber et al.[19] and Papageorgiou et al.[15]

* E-mail: junghaenel@hmi.de. Fax: +49 (030) 8062-2434.

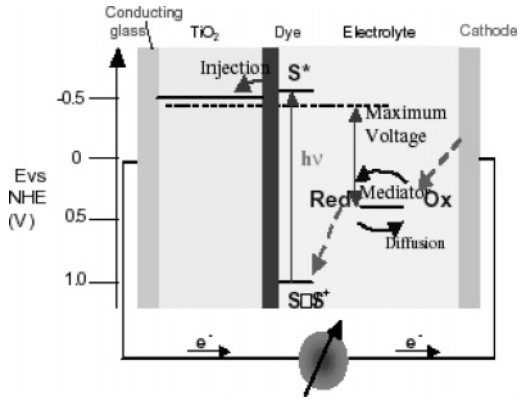

Figure 1. Operation principle of a dye sensitized solar cell (reprinted with permission from ref 29, copyright 2003 Elsevier).

The models proposed do not account for the slower diffusion coefficients in the nanoporous TiO_2 layer as found by other authors.[16] In addition, the impact of the bulk electrolyte layer thickness is believed to be critical for understanding the depletion of both triiodide and iodide in a DSSC under illumination.

Chemically, the cell can be described in terms of a combination of the following reactions: reactions at the front and counter electrode (CE) necessary for the operation of the cell

$$S + h\nu \xrightarrow{k_1} S^{\ddagger} \quad (1)$$

$$S^{\ddagger} \xrightarrow{k_2} TiO_2\,(e^-) + S^+ \quad (2)$$

$$2S^+ + 3I^- \xrightarrow{k_3} I_3^- + 2S \quad (3)$$

$$I_3^- + 2e^-\,(CE) \xrightarrow{k_4} 3I^- \quad (4)$$

10.1021/jp054445r CCC: $30.25
Published on Web 11/11/2005

and unwanted side reactions

$$S^+ \xrightarrow{k_5} P \tag{5}$$

$$I_3^- + 2TiO_2\,(e^-) \xrightarrow{k_6} 3I^- \tag{6}$$

$$2S^{\ddagger} + I_3^- \xrightarrow{k_7} 2S^+ + 3I^- \tag{7}$$

2. Experimental Section

2.1. Materials. Optically transparent conducting glass (F:SnO_2, sheet resistance 10 Ω/□, thickness 2 mm) was purchased from Asahi Glass (Japan). TiO_2 (P25) came from Degussa and was used as received. Ethanol (absolute, Merck), acetonitrile (p.a., Fluka), and isopropanol (p.a., Fluka) were used without further purification and stored over 4 Å molecular sieves. Anhydrous LiI (p.a., Fluka), Triton X (Fluka), I_2 (double sublimated, >99%, Merck), and acetylacetone (p.a., Merck) were also used without special treatment.

2.2. Preparation of the Electrodes. A 12 g portion of TiO_2 (P25) was added to a solution of 62 mL of ethanol, 400 μL of Triton X, and 400 μL of acetylacetone. The suspension was treated in an ultrasonic bath for 90 s to homogenize it. The front electrode was coated with TiO_2 by dipping the FTO glass into the suspension several times. In each cycle, the electrode was dipped, pulled out, and dried at room temperature, so that the layer thickness increased by an average of 2 μm. These plates were used to make lengthy electrodes (typically 4.5×1.5 cm^2) by partially removing the TiO_2 layer with a cloth. After annealing at 450 °C for 45 min, they were transferred into a 1.25×10^{-4} M solution of Ru-535 dye in absolute ethanol at room temperature for 1 day.

The FTO counter electrode was platinized by dropping 25 μL of a 0.5 mM $H_2PtCl_6 \cdot 6H_2O$ solution onto the glass, followed by annealing at 380 °C for 15 min. Both electrodes were clamped together with Surlyn foil, which was placed between the glas plates, heated to 100 °C, and pressed for 3 min at 2 kN. The electrolyte (0.5 M LiI, 0.05 M I_2, 0.2 M 4-*tert*-butylpyridine in acetonitrile) was filled between the electrodes with the vacuum method. The interior of the cell was evacuated, put into the electrolyte, and exposed to room pressure.

Finally, the cell was hermetically sealed with TorrSeal vacuum glue. The solar cell efficiency was in the range of 3−5%, mainly due to the comparatively low average TiO_2 layer thickness (7 μm) and the high internal resistance.

2.3. Methods. The thickness of the TiO_2 layers was determined with a Dektak-Step-Profiler (Sloan Dektak 3030, Veeco Instruments). For all cells described below, it was between 0.8 and 15 μm.

The scanning microscopy for semiconductor devices (SMSC) apparatus was constructed at the Hahn-Meitner-Institut and consists of a red laser (632.8 nm) with a spot diameter between 0.4 and 400 μm. The beam is directed onto the sample that is free to move in two directions. By measuring the photocurrent in a point by point manner, two-dimensional photocurrent images are obtained.

3. Results and Discussion

3.1. Photocurrent Characteristics of DSSCs with a TiO_2 Thickness Gradient. A set of lengthy cells were assembled in which the TiO_2 layer thickness was increased stepwise from 0.8 to 15 μm by a dip-coating technique. DEKTAK measurements revealed that each layer itself was quite planar but that the change from step to step was very inhomogeneous especially for the first layers, which is reflected in the noisy photocurrent signals displayed in Figures 2 and 3. Then, the photocurrent was measured space resolved by SMSC (scanning microscopy for semiconductor devices), a technique in which a small laser spot of about 50 μm × 50 μm with a wavelength of 632.8 nm and a light intensity of 100 mW/cm^2 is directed to the sample. By measuring the photocurrent point by point, two-dimensional photocurrent images are obtained. We can see in Figures 2 and 3 that the initial photocurrent increases linearly from 0.8 to about 10 μm, reaching a maximum, and decreases slightly if the layer thickness is further increased. This is in good agreement with theoretical expectations which predict an increasing photocurrent with increasing dye load due to increasing absorption and electron injection. However, for thicker layers, a decrease of photocurrent is observed because the average path length for the electron diffusion becomes longer and the recombination probability increases.

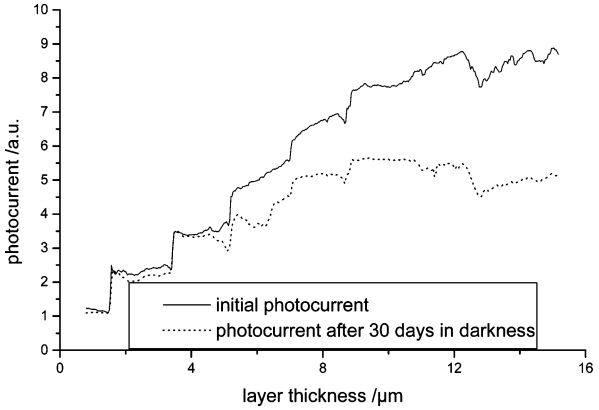

Figure 2. Degradation of a DSSC as a function of layer thickness in darkness.

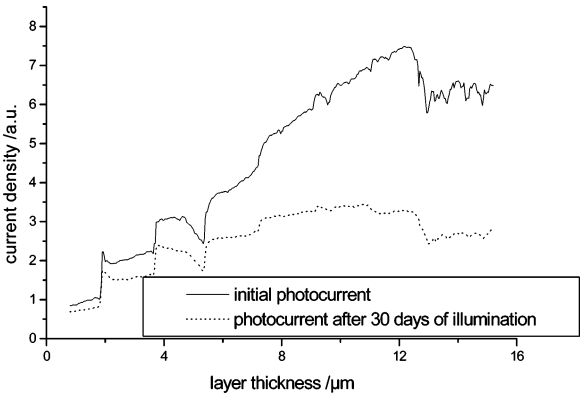

Figure 3. Degradation of a DSSC as a function of layer thickness under illumination.

After illumination under AM 1.5 (Figure 3) or storage in darkness (Figure 2) for 30 days, one can see that the photocurrent decreases significantly especially in the thicker parts. Degradation is an overlap of several independent phenomena; some of them are light-independent, and some of them, light-induced. When looking at Figure 2, we can see that the light-independent degradation (imperfect sealing, water penetration, and electrolyte decomposition) increases more or less linearly with the layer thickness. This is itself an interesting result. It may indicate that the nanoporous structure is subject to changes which are accumulating their effect on solar cell efficiency. Possible reasons may be the clogging of pores, coagulations of nanoparticles, or the formation of microbubbles.

TABLE 1: Typical Parameters for Dye Sensitized Solar Cells Taken from the Literature

	symbol and unit	values found in the literature	used value
concentration of the sensitizer	[S] (mol/L)	for calculation, see section 3.4	0.13
absorption coefficient	ϵ (1/(M cm))	strongly dependent on wavelength; peaks at 1.3×10^4 (518 nm), 1.33×10^4 (380 nm) (ref 20)	1.33×10^4
porosity	Por	0.5 (ref 21), 0.65 (ref 21)	0.6
diffusion coefficient of I^- in nanoporous layer	D_{I^-np} (cm^2/s)		1.3×10^{-6}
diffusion coefficient of I^- in acetonitrile	D_{I^-b} (cm^2/s)		1.3×10^{-5}
diffusion coefficient of I_3^- in nanoporous layer	$D_{I_3^-np}$ (cm^2/s)	2.5×10^{-6} [a] (ref 16)	10^{-6} [a]
diffusion coefficient of I_3^- in acetonitrile	$D_{I_3^-b}$ (cm^2/s)	$>8.5 \times 10^{-6}$ (ref 22), 2.6×10^{-5} (ref 23)	10^{-5}
incident photon to current conversion	IPCE	for explanation, see section 3.3.3	0.4
initial concentration of I^-	$[I^-]_I$ (mol/L)	standard value for most cells	0.45
initial concentration of I_3^-	$[I_3^-]_I$ (mol/L)	standard value for most cells	0.05
thickness of nanoporous layer	l (μm)	optimal value in the range of 10 (ref 24) to 20 (ref 25)	15
total thickness	b (μm)	determined by measuring the thickness of Surlyn foil, a widely used sealant	60

[a] The porosity of the medium was above the typical values (69−83%), and pictures magnified 1500 times revealed a very craggy surface, so one can expect the stated diffusion coefficient to be an upper limit.

The illuminated area of the cell degraded much faster in the cell region where the layer was thick. A photocurrent decrease of 20% is found for a 0.8 μm thick layer, and one of 66% is found for a 12 μm thick layer. It seems that the thicker parts of the cell suffer from an inappropriate iodide support due the limited access of the nanoporous network. This is a very critical point since most of the photocurrent conversion takes place near the front electrodes, at a point where the iodide support may be insufficient. A clarification of this phenomen appears to be critical for operating highly efficient dye solar cells. In the following sections, a simple model is derived to explain the depletion of iodide near the front electrode.

It should be noted that the observed degradation rate is higher than that found by other authors.[31,32] This is due to the use of a different electrolyte, which does not contain any imidazolium derivatives and uses pure acetonitrile as a solvent.

3.2. Conventions

$[I_3^-]_{np}(x)$ = triiodide concentration in the nanoporous TiO_2 layer as a function of x

$[I^-]_{np}(x)$ = iodide concentration in the nanoporous TiO_2 layer as a function of x

$[I_3^-]_b(x)$ = triiodide concentration in the bulk solution as a function of x

$[I^-]_b(x)$ = iodide concentration in the bulk solution as a function of x

x = distance from the FTO contact (μm)

l = thickness of the nanoporous layer (μm)

b = total thickness of the cell (nanoporous layer and thickness of the bulk solution)

IPCE = incident photon to current conversion

P_i = incident light intensity (mol/(m^2 s))

$k = [S]\epsilon \ln(10)$

[S] = concentration of the sensitizer (mol/L)

ϵ = extinction coefficient (1/(M cm))

$[I_3^-]_I$ = initial concentration of triiodide (mol/L)

$[I^-]_I$ = initial concentration of iodide (mol/L)

Por = porosity of the layer

$D_{I_3^-np}$ = diffusion coefficient of triiodide in the nanoporous layer (cm^2/s)

D_{I^-np} = diffusion coefficient of iodide in the nanoporous layer (cm^2/s)

$D_{I_3^-b}$ = diffusion coefficient of triiodide in the bulk solution (cm^2/s)

D_{I^-b} = diffusion coefficient of iodide in the bulk solution (cm^2/s)

Remark: The photocurrent I_{ph} is related to the incident light through

$$I_{ph} = FP_i(\mathrm{IPCE})e^{-kl}$$

where F = the Faraday constant.

3.3. Assumptions. *3.3.1. Light Absorption.* It is assumed that the light absorptions in the cell obey Lambert−Beer's law. That means that any absorption through the electrolyte is neglected, no photon loss at the various interfaces within the cell is permitted, and any interaction between the dye molecules is not taken into account. The law is restricted to monochromatic light and does not include any scattering processes at the nanoparticles. However, all these simplifications do not have any major influence on the exponential decay of light absorption with increasing layer thickness, which is believed to be critical for the understanding of transport phenomena in the nanoporous TiO_2 layer. For a well-injecting sensitizer, the absorption of light is directly proportional to the generation rate of I_3^- and the consumption rate of I^- and, if one assumes a homogeneous distribution of the dye molecules in the TiO_2 layer, the Lambert−Beer Law is suitable to describe the I_3^-/I^- generation/consumption in a DSSC. The model distinguishes between two cases: illumination through the front electrode (FE) and through the counter electrode (CE), the first one being of special interest because it describes the common operation mode of the cell.

3.3.2. Driving Force for Mass Transport. The model assumes diffusion to be the only transport process for I_3^-/I^- ions in the cell. It seems to be reasonable to disregard convection as a source of mass transport especially in the nanoporous layer with its small pores, since the temperature gradient within the cell is small at steady-state conditions. Migration, however, might be a force that contributes to some extent, but as calculations have shown,[15] the contribution to the total transport is small and might be neglected.

In bulk solution (the distance between the nanoporous TiO_2 layer and the CE), a purely diffusional model can be considered to be quite accurate, whereas in the nanoporous layer the morphology and kinetics of the system are analogous to those in liquid chromatography columns. The molecules adsorb and desorb constantly on the TiO_2 surface. Since an activation energy $\Delta G^{\ddagger}$ is needed for the molecule to desorb, the mass transport rate will include a term $-\Delta G^{\ddagger}/kT$ and therefore strongly depends on the temperature. Furthermore, other transport mechanisms on the surface itself might play a role as well. For the sake of simplicity, first, we considered only unhindered diffusion in the nanoporous layer and approximated all the interaction processes with a modified diffusion constant that is 1 order of magnitude smaller than that used in homogeneous solution as suggested by Kebede and Lindquist.[16]

3.3.3. Other Assumptions. The model does not account for the structure of the nanoporous TiO_2 layer. It is treated as a pseudo-homogeneous medium in which the electrolyte diffuses more slowly but is essentially unhindered. Pores with limited access or the thin passages from one pore to another are not described. One could try to simulate the nanoporous layer as a randomly distributed assembly of ball-shaped TiO_2 particles, but then, one would have to develop a two- or three-dimensional model, which would most likely not be so easily interpreted.

The whole process of absorption, electron injection, electron transport, and recombination reaction is described by one parameter, IPCE. This is the probability that a given photon is converted to an electron which runs through the outer electric circuit and is able to perform work. Its value was adjusted in a way that the photocurrent matches properly working cells with efficiencies of about 10%. This simplification is certainly not justified if one would try to understand *I*/*V* curves, but since we are only interested in the place where the redox reactions of the electrolyte take place, a more detailed description would not affect our model in a significant way.

3.4. Parameters Used for the Model. See Table 1 for details and values used. The calculation of the sensitizer concentration can be written as follows:

$$[\mathrm{S}] = \Gamma A_{\mathrm{TiO_2}} \rho_{\mathrm{TiO_2}} (1 - \mathrm{Por})$$

Table 2 lists the definitions and values of the above parameters.

TABLE 2

	symbol and unit	used value
surface area of TiO_2	A_{TiO_2} (m^2/g)	50 (derived from average particle diameter $d = 25$ nm)
density of TiO_2	ρ_{TiO_2} (g/cm^3)	4.2
surface concentration of sensitizer	Γ (mol/cm^2)	1.3×10^{-7} (ref 26)

3.5. Model for I_3^-/I^- Mass Transport in Nanoporous TiO_2 and Bulk Solution. *3.5.1. General Differential Equation for Mass Transport in the Nanoporous Layer and the Bulk Solution Based on a Diffusion Model.* An analytical formula is derived that describes the concentration of I_3^-/I^- with respect to the distance from the FTO contact. The point $[I_3^-](0)$ and $[I^-](0)$ refers to the concentration at the FTO/TiO_2 interface, the point $x = l$, to the nanoporous TiO_2/bulk solution interface, and the point $x = b$, to the counter electrode. The model is based on Fick's second law under steady-state conditions.

$$D_{\mathrm{I_3^-np}} \frac{\mathrm{d}^2[\mathrm{I_3^-}]_{\mathrm{np}}(x)}{\mathrm{d}x^2} + \frac{1}{2}\mathrm{IPCE}\,\frac{\mathrm{d}}{\mathrm{d}x} P_{\mathrm{i}} \mathrm{e}^{-kx} = 0$$

Triiodide

$$D_{\mathrm{I^-np}} \frac{\mathrm{d}^2[\mathrm{I^-}]_{\mathrm{np}}(x)}{\mathrm{d}x^2} - \frac{3}{2}\mathrm{IPCE}\,\frac{\mathrm{d}}{\mathrm{d}x} P_{\mathrm{i}} \mathrm{e}^{-kx} = 0 \qquad (1)$$

Iodide

$$\frac{\mathrm{d}^2[\mathrm{I_3^-}]_{\mathrm{b}}(x)}{\mathrm{d}x^2} = 0$$

Triiodide

$$\frac{\mathrm{d}^2[\mathrm{I^-}]_{\mathrm{b}}(x)}{\mathrm{d}x^2} = 0 \qquad (2)$$

Iodide

Equations 1 and 2 refer to a steady-state condition where no change of iodide/triiodide concentration with respect to time and place occurs (Fick's second law). In bulk solution (eq 2), the slope of the concentration gradient is constant, since no wells or sinks for the regarded molecules have to be considered. In the nanoporous layer (eq 1), however, the dye is oxidized upon excitation by light and initiates a redox reaction with the electrolyte.

$$2\mathrm{dye}^+ + 3\mathrm{I}^- \rightarrow 2\mathrm{dye} + \mathrm{I_3}^-$$

That means that iodide is consumed ($-^3/_2$ molecules per dye) and triiodide is created ($+^1/_2$ molecule per dye) in the nanoporous layer depending on the incident light intensity (P_i) and the incident photon to current conversion (IPCE).

The generation of iodide/triiodide molecules is assumed to be directly proportional to the incident light intensity. That means that with a constant probability every photon that is absorbed causes the injection of an electron. With this assumption, we can use the very simple law of Lambert and Beer to describe the injection process with respect to distance from the front contact.

3.5.2. General Solutions of the Differential Equations. The following are solutions to eqs 1 and 2 for $k = [\mathrm{S}]\epsilon\ \ln(10)$:

Solutions to eq 1

$$[\mathrm{I_3^-}]_{\mathrm{np}}(x) = -\frac{1}{k^2} a \mathrm{e}^{(-kx)} + c_1 x + c_2$$

Triiodide

$$[\mathrm{I^-}]_{\mathrm{np}}(x) = -\frac{1}{k^2} a \mathrm{e}^{(-kx)} + c_1' x + c_2' \qquad (3)$$

Iodide

$$a = \frac{1}{D_{\mathrm{I^-np}}} \frac{1}{2} (\mathrm{IPCE}) P_{\mathrm{i}} k$$

Triiodide

$$a' = \frac{1}{D_{\mathrm{I^-np}}} \frac{1}{2} (\mathrm{IPCE}) P_{\mathrm{i}} k \qquad (4)$$

Iodide

Solutions to eq 2

$$[\mathrm{I_3^-}]_{\mathrm{b}}(x) = c_3 x + c_4$$

Triiodide

$$[\mathrm{I^-}]_{\mathrm{b}}(x) = c_3' x + c_4' \qquad (5)$$

Iodide

One can see that four independent equations are needed to determine the variables c_1/c_1', c_2/c_2', c_3/c_3', and c_4/c_4'.

3.5.3. Boundary Conditions.

(1) Concentration at the TiO_2/bulk solution interface

$$[\mathrm{I_3^-}]_{\mathrm{np}}(l) = [\mathrm{I_3^-}]_{\mathrm{b}}(l)$$

Triiodide

$$[\mathrm{I^-}]_{\mathrm{np}}(l) = [\mathrm{I^-}]_{\mathrm{b}}(l) \qquad (6)$$

Iodide

Equation 6 refers to the interface between the nanoporous layer and the bulk solution (distance $x = l$). Under steady-state conditions, the concentration at this point has to be the same on both sides.

(2) Flux of triiodide and iodide at the FTO contact

$$\left[\frac{\partial[I_3^-]_{np}}{\partial x}\right]_{x=0} = 0 \quad \text{Triiodide}$$

$$\left[\frac{\partial[I^-]_{np}}{\partial x}\right]_{x=0} = 0 \quad \text{Iodide} \tag{7}$$

At the front electrode, the transport of I_3^-/I^- has to be zero because the system is closed. Using Fick's first law, which describes mass transport (dn/dt) in terms of a concentration gradient (dc/dx), this differential equation has to be zero for both I_3^- and I^- (eq 7).

(3) Conservation of triiodide and iodide

$$\text{Por}\int_0^l [I_3^-]_{np}(x)\,dx + \int_l^b [I_3^-]_b(x)\,dx = [I_3^-]_I l(\text{Por}) + [I_3^-]_I(b-l) \quad \text{Triiodide}$$

$$\text{Por}\int_0^l [I^-]_{np}(x)\,dx + \int_l^b [I^-]_b(x)\,dx = [I^-]_I l(\text{Por}) + [I^-]_I(b-l) \quad \text{Iodide} \tag{8}$$

*In the nanoporous layer, the porosity (*Por*) has to be considered because the electrolyte occupies only the pores of the TiO_2*

Equations 8 say that the total amount of I_3^- and I^-, respectively, has to be conserved. If one was more precise, one would have to say that the sum of iodide and triiodide molecules with their stoichiometry factors has to be constant at all times, since they are related through a redox equilibrium. However, it is hard to assess how the initial concentration of I_3^-/I^- changes in the steady-state situation. So, we arbitrarily assume that the initial concentration does not change at all.

This equation is integrated over the nanoporous layer (from 0 to l) and the bulk solution (from l to b).

(4) Mass transport at the TiO_2/bulk solution interface

$$D_{I^-np}\left[\frac{\partial[I_3^-]_{np}}{\partial x}\right]_{x=1} = D_{I^-b}\left[\frac{\partial[I_3^-]_b}{\partial x}\right]_{x=1} \quad \text{Triiodide}$$

$$D_{I^-np}\left[\frac{\partial[I^-]_{np}}{\partial x}\right]_{x=1} = D_{I^-b}\left[\frac{\partial[I^-]_b}{\partial x}\right]_{x=1} \quad \text{Iodide} \tag{9}$$

The fluxes of I_3^-/I^- molecules have to be the same at the interface between the nanoporous layer and the bulk solution. Using Fick's first law and under consideration of the different diffusional constants in the nanoporous layer and the bulk solution, one obtains eq 9.

3.5.4. Algebraic Conversion. Equations 1 and 2 can be solved analytically using partial integration and basic algebraic conversion. One obtains the following constants for eqs 3 and 5:

$$c_1 = -\frac{a}{k} \quad \text{Triiodide}$$

$$c_1' = -\frac{a}{k} \quad \text{Iodide}$$

$$c_2 = [I_3^-]_I + \frac{1}{[(\text{Por})l + b - l]}\left(\frac{a(\text{Por})(1-e^{-kl})}{k^3}\right) + \frac{a(\text{Por})l^2}{2k} - \frac{1}{2}c_3(b^2-l^2) + \left(c_3 l + \frac{a(e^{-kl}+kl)}{k^2}\right)(b-l) \quad \text{Triiodide}$$

$$c_2' = [I^-]_I + \frac{1}{[(\text{Por})l + b - l]}\left(\frac{a(\text{Por})(1-e^{-kl})}{k^3}\right) + \frac{a(\text{Por})l^2}{2k} - \frac{1}{2}c_3(b^2-l^2) + \left(c_3 l + \frac{a(e^{-kl}+kl)}{k^2}\right)(b-l) \quad \text{Iodide}$$

$$c_3 = \frac{a(e^{-kl}-1)}{k}\frac{D_{I_3^-np}}{D_{I-b}} \quad \text{Triiodide}$$

$$c_3' = \frac{a(e^{-kl}-1)}{k}\frac{D_{I^-np}}{D_{I-b}} \quad \text{Iodide}$$

$$c_4 = c_2 - \frac{ae^{-kl}}{k^2}(1+kl) \quad \text{Triiodide}$$

$$c_4' = c_2 - \frac{ae^{-kl}}{k^2}(1+kl) \quad \text{Iodide} \tag{10}$$

3.5.5. Application of the Formula. Using typical values taken from the literature as indicated in Table 1, one obtains a concentration distribution, as shown in Figure 4. The photocurrent of the modeled cell would be 19.5 mA/cm^2, yielding a cell with an efficiency of about 10%. One should notice that the concentration gradient on average is much higher in the nanoporous layer than in the bulk solution, reflecting the smaller diffusion coefficient. The I^- concentration reaches a minimum at the front contact and is only 30% of its initial value. On the other side, I_3^- accumulates and its concentration rises to 370% of the initial value. This means that the effective concentration ratio of I^-/I_3^- changes by $0.3/3.7 = 0.08$, that is by more than 1 order of magnitude. The redox potential, thus, shifts positively by ca. 60 mV. This is equivalent to an effective I^- concentration of 0.05 M. According to Fick's first law, the mass transport is proportional to the concentration gradient. To sustain an equal mass transport for I_3^- and I^-, the relative I_3^- concentration change has to be much higher than the iodide concentration change because the total amount of I_3^- is only about 10% of I^-. That is the reason that the I_3^- concentration drops to 33% at the counter electrode, whereas the I^- concentration only rises to 117%.

One of the major conclusions that can be derived from these calculations under standard conditions is that the I^- concentration depletes to the same extent as the I_3^- concentration does, although there is a large excess of iodide present and the diffusion coefficient is assumed to be 1.3 times higher than that of triiodide. Up to now, only triiodide has been suspected to be critical for charge transport limitations[15,16,19] and the role of iodide has not been investigated to any further extent. None of the formulas modeling the mass transport of the electrolyte so far[15,19] include both the existence of a bulk solution and different diffusion coefficients in the nanoporous layer and the bulk solution. Especially, the thickness of the bulk layer has a great effect on the depletion of the I_3^-/I^- concentration and, therefore,

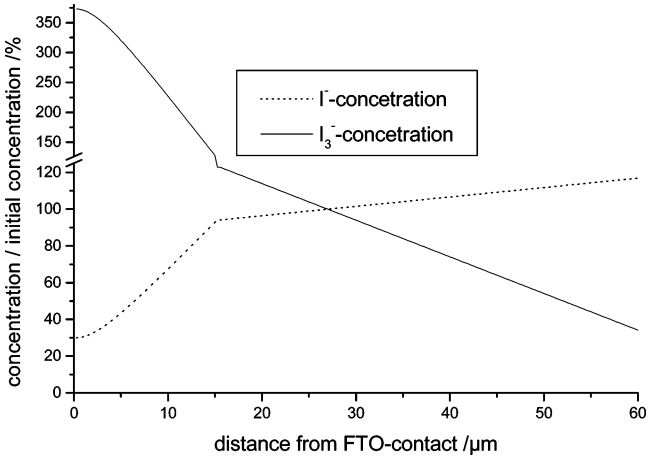

Figure 4. Concentration gradient of the electrolyte under steady-state conditions.

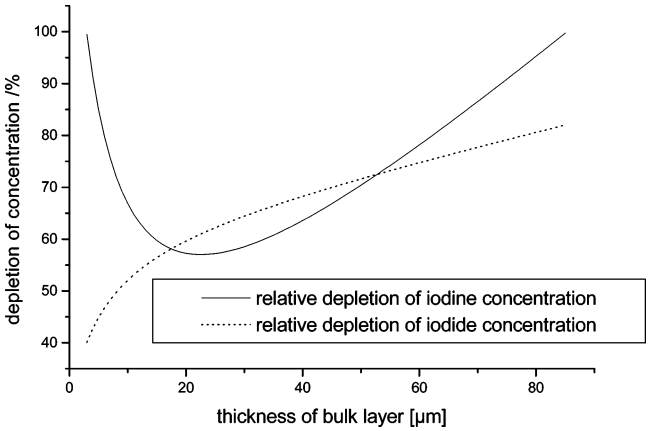

Figure 5. Maximum depletion of the electrolyte concentration as a function of the bulk layer thickness.

on the maximum photocurrent that can be obtained if diffusion is limiting. Figure 5 shows the maximum depletion of the I_3^-/I^- concentration as a function of the bulk electrolyte layer thickness. The lowest I^- concentration is always measured at the front electrode, and the lowest I_3^- concentration, at the counter electrode.

To understand these results, it is best to imagine a cell without any bulk electrolyte layer at all. In such a cell, the I^- concentration at the counter electrode would be higher than its initial value, and the I_3^- concentration, lower. Now, if one adds a bulk layer with the initial electrolyte concentration, I^- ions would diffuse into the bulk layer and, in order to maintain the same transport rate in the nanoporous layer (which is proportional to dc/dx), the concentration is shifted downward by a certain offset at every point. Since this includes the front contact as well, the maximum depletion of iodide increases with increasing bulk layer thickness. The same argument can be used to explain the I_3^- curve up to 20 μm of bulk layer thickness. If one increases the bulk layer further, another effect comes into play: the resistance of the bulk layer itself becomes rate limiting, since the concentration gradient needed to support a certain transport rate increases with increasing layer thickness.

In conclusion, there exists a bulk layer thickness for which the maximum depletion of the I_3^-/I^- concentration reaches a minimum, which is wanted in terms of higher photocurrents and lower degradation rates.

(A) Illumination from the Back Electrode. From time to time, the question is asked, what impact does the illumination direction have on the cell performance? Due to the absorption

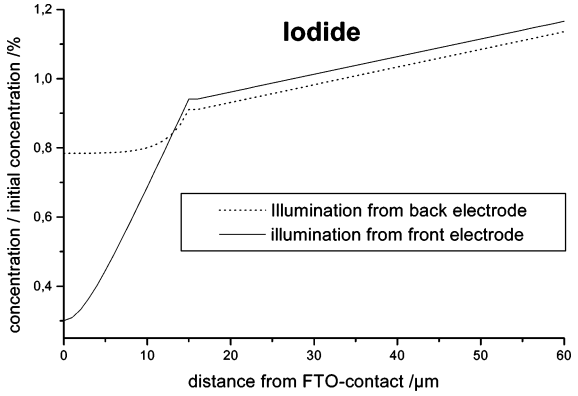

Figure 6. Concentration distribution of iodide for different illumination directions.

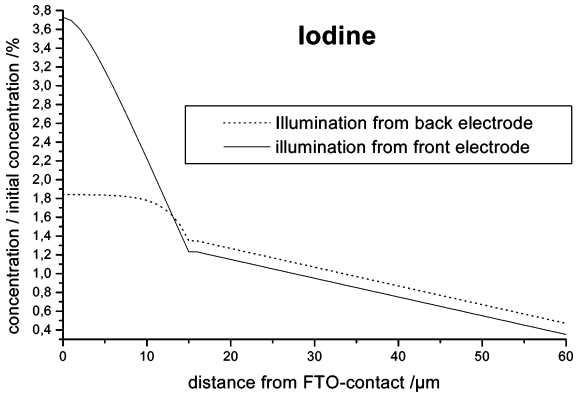

Figure 7. Concentration distribution of triiodide for different illumination directions.

of the electrolyte, some of the incident light is absorbed and usually the efficiency of the cell is decreased on the order of 10−20%. However, from the point of electrolyte diffusion, an illumination from the counter electrode is desirable because the average path length the I_3^-/I^- molecules have to travel is reduced. On the other hand, injected electrons have to migrate over a longer distance. Due to the exponential decay of absorption as described by the Lamber−Beer Law, most of the charge carriers are generated at the point where the light hits the surface first. It can be seen in Figures 6 and 7 that this has a great effect on the concentration distribution. Most importantly, the concentration of iodide, which is believed to be critical for the long-term stability of a DSSC, is increased by a factor of 2 at the front electrode.

(B) Advanced Model Including Adsorption/Desorption Steps in the Nanoporous Layer. The presented model assumes unhindered diffusion in the nanoporous TiO_2 layer as if it was a homogeneous medium. This is, of course, a very rough description, and a more precise model would be desirable, particularly as the applied diffusion coefficient contains an error bar which can be estimated to be in the range of 1 order of magnitude. However, at the same time, it has a great impact on the concentration distribution. Apparently, the situation in the nanoporous layer differs a lot from the situation in the bulk solution. I_3^-/I^- molecules can adsorb/desorb on the TiO_2 surface with a certain sorption heat ΔG, which is a function not only of temperature but also of the concentration of the concerned molecule/ion, of the concentration of the molecules/ions in the surrounding area, and of the surface properties of TiO_2. To our knowledge, no simulation of isotherms have been done for nanoporous TiO_2, but much knowledge has been gathered on alkanes sorption on zeolites, applying kinetic Monte Carlo

simulations.[30] Besides this hopping mechanism, that consists of diffusion in the solvent, adsorption on the TiO_2 surface for a certain time, desorption, and so on, one would also have to estimate the contribution of surface diffusion. Surface diffusion is at first approximation proportional to the unoccupied surface states, which may be hard to calculate on the sensitized TiO_2 layer. Nevertheless, more extended theoretical work may provide good access to this critical parameter of mass transport, which is essential for a better approximation of the maximum attainable photocurrent and of degradation phenomena.

3.6. Degradation Phenomena in Dye Sensitized Solar Cells Due to Low I^- Concentration. In the previous section, we have seen that both the I^- and I_3^- concentrations may significantly deplete/accumulate in the nanoporous layer. This has an influence on the redox potential of the electrolyte (which is shifted to more positive values by up to 60 mV) and on the maximum attainable photocurrent. In the case of I^-, an additional question arises: what is the effect on the sensitizer regeneration? It is known from theoretical modeling that the regeneration of the oxidized dye molecule has to be 8 orders of magnitude faster than any competitive degeneration reaction.[27] This means that it must be ensured that enough reducing agent, I^-, is present at every point in the cell, which might not be the case near the front contact. Assuming first-order kinetics for the sensitizer degradation and neglecting all other degradation phenomena due to imperfect sealing, electrolyte decomposition, and degradation processes in the dark and at elevated temperatures,[28] one obtains the following formula for the time at which half of the sensitizer is consumed:[27]

$$T_{1/2} = \frac{\ln 2[\mathrm{S}]k_3}{\mathrm{IPCE}k_5}\frac{\mathrm{I}^-}{P_\mathrm{i}} \tag{11}$$

In this formula, [S] is the sensitizer concentration, k_3 is the rate constant for the regeneration of the sensitizer, and k_5 is the rate constant for the irreversible product formation. It is shown that the lifetime is critically determined by the local I^- concentration. In addition, it is also dependent on the concentration of the sensitizer, which can act as a buffer, when available in excess. Unfortunately, little is known about the light-induced decomposition reaction itself. High-performance liquid chromatography (HPLC) measurements indicate a variety of different products which are, however, difficult to identify.

The photochemistry of I_2 itself might contribute to the degradation of the sensitizer. Below a 500 nm wavelength, I_2 dissociates into reactive $I^\bullet$ radicals, which can induce side reactions with the sensitizer.

Equation 11 provides a direct link between stability and iodide concentration. Both parameters are directly proportional to each other, which implies that in a cell with only half the iodide concentration the sensitizer will degrade two times faster. That reflects the importance of the oxidized sensitizer molecule for degradation. If for some reason (plugged pores, hindered diffusion) the iodide concentration is low, the sensitizer has to remain in the oxidized state for a longer time period and is, thus, more susceptible to an irreversible reaction. Our calculations in the previous chapter have shown that, for normal cell operations, the iodide concentration may decrease to 30% of its initial value at the front electrode, which implies that the degradation rate in this part of the cell is about three times faster. However, one has to keep in mind that photoinduced side reactions are only one part of the overall degradation of a DSSC and that it is difficult to assess to what percentage they contribute. Based on our experiments and experiments done before,[28] eq 11 gives a good qualitative description of the cell lifetime but, since it does not include other degradation phenomena (e.g., electrolyte bleaching, imperfect sealing, etc.), it may not be sufficient for analysis. A very critical parameter might also be the special geometry of the nanoporous TiO_2 particles. If pores are completely or almost completely blocked, they are not accessible to the electrolyte anymore, and on the other hand, cracks within the layer may provide channels through which the electrolyte may diffuse very easily. None of these situations have entered the model although they may locally influence the I^- concentration very strongly. An improved model would have to apply the percolation theory to account for the porous material.

4. Conclusion

Iodide was confirmed to play a crucial role both in the maximum attainable photocurrent and in degradation phenomena even in nominally high concentration (0.5 M). Modeling the mass transport in DSSCs revealed that for a 10% efficient cell using typical parameters the iodide concentration depletes to 30% of its initial value at the front electrode. However, the mass transport rate in the nanoporous TiO_2 layer is greatly affected by the diffusion coefficient of I^- and I_3^-, and the accuracy of the model is therefore limited. More experimental effort has to be undertaken to gather additional information about the diffusion rate in the nanoporous layer and the underlying mechanisms. The large surface area of 50 m^2/g suggests that adsorption/desorption steps have a significant effect on the transport mechanism, which should be taken into account since the temperature dependence on the diffusion coefficient would be at least partly exponential and not linear as in the bulk solution.

The electrolyte bulk layer between the back electrode and the TiO_2 has so far only been considered as a resistor that prevents direct electron transfer to the back electrode, and when modeling a DSSC, it is usually assumed to be zero. Now, it turns out that it has a significant effect on the maximum attainable photocurrent and that the optimum layer thickness is in the range of ca. 20 μm. This has little influence on practical implementation, since most DSSCs have these layer thicknesses due to technical limitations anyway, but one should note that the maximum cell efficiency is not obtained with a negligibly small bulk layer.

The role of I^- as a regenerating agent for the oxidized state of the dye was examined in long-term experiments. It turned out that thicker TiO_2 layers degrade faster, which is consistent with the model derived. In the thick TiO_2 layers, iodide diffusion is hindered because of the narrow nanoporous network so that the iodide concentration at the front electrode is only about 30% of its initial value. Thus, the average time in which the dye remains in its oxidized state is prolonged and decomposition reactions are enhanced.

Highly (10%) efficient solar cells with 15 nm TiO_2 layer thicknesses are experiencing a 70% reduction (from 0.5 M) of iodide concentration within the porous TiO_2 structure near the front contact, which may explain the observed photodegradation phenomenon. Contradicting theoretical[15,16] and experimental[18] results on long-term stability may still be explained on the basis of a surplus of the sensitizer S, which may gradually be consumed throughout the TiO_2 layer, while suggesting temporal stability.

References and Notes

(1) Hagfeldt, A.; Grätzel, M. *Chem. Rev.* **1995**, *95*, 49.
(2) Grätzel, M. *J. Photochem. Photobiol., C* **2003**, *4*, 145.

(3) McConnell, R. D. *Renewable Sustainable Energy Rev.* **2002**, *6*, 273.

(4) Polo, S. A.; Itokazu, M. K.; Murakami Iha, N. Y. *Coord. Chem. Rev.* **2004**, *248*, 1343.

(5) Campbell, W. M.; Burrell, A. K.; Officer, D. L.; Jolley, K. W. *Coord. Chem. Rev.* **2004**, *248*, 1363.

(6) Liu, Y.; Hagfeldt, A.; Xiao, X. R.; Lindquist, S. E. *Sol. Energy Mater. Sol. Cells* **1998**, *55*, 267.

(7) Kusama, H.; Konishi, Y.; Sugihara, H.; Arakawa, H. *Sol. Energy Mater. Sol. Cells* **2003**, *80*, 167.

(8) Wang, P.; Zakeeruddin, S. M.; Comte, P.; Exnar, I.; Grätzel, M. *J. Am. Chem. Soc.* **2003**, *125*, 1166.

(9) Nelson, J. *Phys. Rev. B: Condens. Matter* **1999**, *59* (12), 15374.

(10) Schwarzburg, K.; Willig, F. *J. Phys. Chem. B* **1999**, *103*, 5743.

(11) Yoshida, T.; Pauporte, T.; Lincot, D.; Oekermann, T.; Minoura, H. *J. Electrochem. Soc.* **2003**, *150* (9), C608.

(12) Moeckel, H.; Giersig, M.; Willig, F. *J. Mater. Chem.* **1999**, *9*, 3051.

(13) Tennakone, K.; Kumara, G. R. R. A.; Kottegoda, I. R. M.; Perera, V. P. S. *Chem. Commun.* **1999**, 15.

(14) Sayama, K.; Sugihara, H.; Arakawa, H. *Chem. Mater.* **1998**, *10*, 3825.

(15) Papagerpgiou, N.; Grätzel, M.; Infelta, P. P. *Sol. Energy Mater. Sol. Cells* **1996**, *44*, 405.

(16) Kebede, Z.; Lindquist, S.-E. *Sol. Energy Mater. Sol. Cells* **1998**, *51*, 291.

(17) Kubo, W.; Murakoshi, K.; Kitamura, T.; Yoshida, S.; Haruki, M.; Hanabusa, K.; Shirai, H.; Wada, Y.; Yanagida, S. *J. Phys. Chem. B* **2001**, *105*, 12809.

(18) Kubo, W.; Kambe, S.; Nakade, S.; Kitamura, T.; Hanabusa, K.; Wada, Y.; Yanagida, S. *J. Phys. Chem. B* **2003**, *107*, 4374.

(19) Ferber, J.; Stangl, R.; Luther, J. *Sol. Energy Mater. Sol. Cells* **1998**, *53*, 29.

(20) Grätzel, M. *J. Photochem. Photobiol., C* **2003**, *4*, 145.

(21) Grätzel, M. *J. Photochem. Photobiol., A* **2004**, *164*, 3.

(22) Papagerogiu, N.; Athanassov, Y.; Armand, M.; Bonhote, P.; Petterson, H.; Azam, A.; Grätzel, M. *J. Electrochem. Soc.* **1996**, *143*, 3099.

(23) Popov, A. I.; Rygg, R. H.; Skelly, N. E. *J. Am. Chem. Soc.* **1956**, *78*, 5740.

(24) Dai, S.; Weng, J.; Sui, Y.; Shi, C.; Huang, Y.; Chen, S.; Pan, X.; Fang, X.; Hu, L.; Kong, F.; Wang, K. *Sol. Energy Mater. Sol. Cells* **2004**, *84*, 125.

(25) Itoa, S.; Kitamurab, T.; Wadab, Y.; Yanagidab, S. *Sol. Energy Mater. Sol. Cells* **2003**, *76*, 3.

(26) O'Regan, B.; Grätzel, M. *Nature* **1991**, *353*, 737.

(27) Tributsch, H. *Appl. Phys. A* **2001**, *73*, 305.

(28) Macht, B.; Turrion, M.; Barkschat, A.; Salvador, P.; Ellmer, K.; Tributsch, H. *Sol. Energy Mater. Sol. Cells* **2002**, *73*, 163.

(29) Grätzel, M. *J. Photochem. Photobiol., C* **2003**, *4*, 145.

(30) Smit, B.; Maesen, T. *Nature* **1995**, *374*, 42.

(31) Hinsch, A.; Kroon, J. M.; Kern, R.; Ihlendorf, I.; Ferber, J. *Prog. Photovoltaics* **2001**, *9*, 425.

(32) Wang, P.; Zakeeruddin, S. M.; Humphrey-Baker, R.; Moser, J. E.; Grätzel, M. *Adv. Mater.* **2003**, *15*, 2101.